

# Far from Equilibrium Pulsed Poled Mn-Doped Relaxor Ferroelectrics: A Positive Aging Relaxation Process

Michael W. Mervosh<sup>ab</sup>, Clive A. Randall<sup>ab</sup>

a. Department of Materials Science and Engineering, The Pennsylvania State University, University Park, PA, 16802, USA.

b. The Center for Dielectrics and Piezoelectrics, Materials Research Institute, Millenium Science Complex, University Park, PA, 16802, USA.

Corresponding author: Michael W. Mervosh; mwm6270@psu.edu; N-244, Millennium Science Complex, University Park, PA, 16802, USA

## Abstract

The aging behavior of high temperature pulse poled (HTPP) Mn-doped relaxor ferroelectrics was investigated. It was found that following HTPP, a far from equilibrium state can be realized. Within this state, the dielectric and piezoelectric properties increased with aging in both single crystal and textured ceramic materials. The degree of aging as well as the time scales involved surpassed previous aging studies. The single crystals experienced 40-60% increases over the span of a month, and the textured ceramics experienced 15-20% increases over multiple weeks. Changes in Rayleigh analysis, heat flow at phase transitions, and X-ray diffraction patterns pointed towards an intrinsic transformation in the systems induced by HTPP. It is hypothesized that such a transformation can arise due to far-from-equilibrium conditions driven by the ultra-fast field switching of pulse poling. The resultant uncompensated depolarization field that forms from ineffective bulk screening depressed properties on day one. With time, the defect dipoles within the Mn-doped systems are assumed to align to generate an internal field to counteract the incomplete compensation of the depolarization field. The pulse poled state and the associated positive aging properties were analyzed under a first order elastic Gibbs Landau-Devonshire Theory and other phenomenological descriptions. The HTPP induced internal electric field and electrostrictive coupling lead to the time dependent evolution of a first order ferroelectric transition.

## 1. Introduction

Ferroelectric materials contain a switchable spontaneous polarization,  $P_s$ , that forms below a transition from a high temperature paraelectric phase at the Curie Temperature ( $T_c$ ) [1], [2]. Relaxor ferroelectrics differ somewhat from normal ferroelectrics due to the diffuse nature of their phase transitions and their spontaneous polarization characteristics [3], [4], [5], [6]. While a normal ferroelectric will display a sharp maximum in permittivity at  $T_c$ , relaxors possess a more dispersive transition with a shifting  $T_{max}$  based on their temperature and frequency dependent dynamics [7]. This behavior has been attributed to the existence of localized polar nanoregions, their size

distributions, and the compositional order/disorder within the lattice at nano length scales. [4], [5], [7], [8], [9]. On applying an external electric field to a relaxor, the restructuring of nano-polar domains into a macrodomain state can occur and provide a remanent polarization ( $P_r$ ), overriding local lattice and thermal perturbations that limit the long-range order of the spontaneous polarization [10], [11]. The  $P_r$  of a relaxor material will survive to some extent above  $T_c$  and gradually decay to zero. This contrasts with the sharp, discontinuous drop in  $P_r$  expected from normal ferroelectrics emblematic of a first order ferroelectric transition [3], [5], [12]. Due to the unique characteristics of relaxors, they have enhanced dielectric and electromechanical properties and thereby find use in dielectrics for multilayer capacitors, electrostrictive actuators, piezoelectric transducers, and electro-optics [3], [13], [14], [15], [16]. The electromechanical properties of relaxor ferroelectrics coupled with the scalability of manufacturing into both single crystal and textured ceramics have led to commercial opportunities over traditional polycrystalline  $Pb(Zr,Ti)O_3$  based piezoelectrics [17], [18], [19], [20].

When cooled from  $T_c$  in the absence of an external electric field or a stress gradient, ferroelectrics possess small regions of uniform spontaneous polarization known as domains whose polarization directions are linked to the crystal symmetry of the paraelectric and ferroelectric phases [21], [22]. Under such cooling, these domains are organized randomly with respect to each other to balance the depolarization and elastic energies with the surface energy associated with domain walls [23], [24]. Upon the application of an external electric field of sufficient strength, these domains will begin to align or nucleate new domains to best minimize the electrostatic energy under domain switching in a process known as poling [25], [26], [27]. Conventional direct current poling (DCP) applies an electric field in one direction above a minimum field referred to as the coercive field ( $E_c$ ) and often occurs at elevated temperatures to aid in the mobility of domains [24], [27]. Once a ferroelectric material is poled, it is capable of exhibiting both pyroelectric and piezoelectric properties, the latter of which features a coupling between mechanical and electrical energy [25]. The poling process is an essential step when ferroelectrics require such properties, and there have been several efforts in recent years to improve the poling capabilities of DCP.

One such process meant to outpace DCP is pulse poling [28]. Pulse poling subjects samples to short pulses of electric field in rapid succession and has mostly been used to periodically pole lithium niobate for optical applications [29]. An earlier study in our group (Yu et al.) showed the ability to improve the piezoelectric properties of rhombohedral perovskite relaxor based  $Pb(Zn_{1/3}Nb_{2/3})O_3$ - $PbTiO_3$  single crystal samples by about 30% using  $10\mu s$  pulses [28]. More recent efforts into pulse poling have seen greater improvements in properties relative to DCP through a 2-stage pulsing landscape (as high as 65-75%) [Manuscript Submitted for Publication]. The Yu et al. study along with previous lithium niobate studies reported observations of dendritic domains in their samples resulting from pulse poling [28], [29], [30]. Other pulse poling efforts employing wider pulse widths (0.1-0.2s) have not reported these dendritic domains, thereby suggesting a more conventional ferroelectric domain state [31], [32]. As described by Shur et al., dendritic domains in  $LiNbO_3$  are likely to form if there is ineffective screening of the depolarization field [29], [33].

Such a field arises from the complex field dynamics that develop during poling as described in Figure 1 [33].

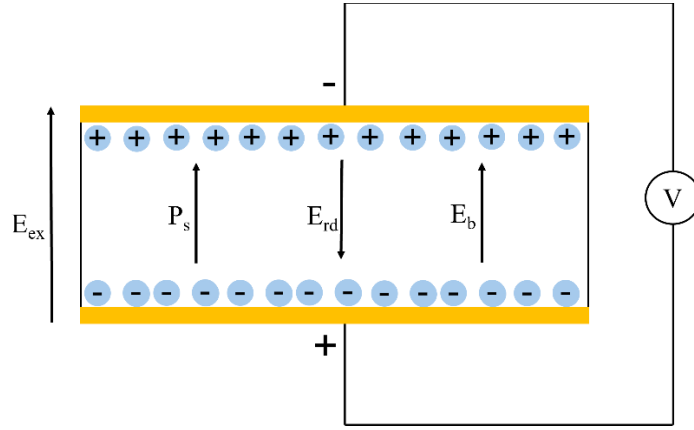


**Figure 1: Field dynamics during poling process**

Figure 1 shows the competing effects of the applied external field ( $E_{ex}$ ), bulk screening field ( $E_b$ ), and residual depolarization field ( $E_{rd}$ ). The expression for  $E_{rd}$  is given by [34]:

$$E_{rd} = -\frac{P}{\epsilon_0 \epsilon_r} \quad (1.1)$$

where  $P$  is polarization,  $\epsilon_0$  is the permittivity of free space, and  $\epsilon_r$  is the relative permittivity of the material. The negative sign indicates that the field forms opposite to the polarization vector. These accumulated and interacting contributions will determine the magnitude of the local electric field in each region which dictates whether a favorable domain will nucleate [29], [33]. The degree to which the depolarization field is screened is described by  $R$ , the ratio between the field switching rate ( $1/t_s$ ) and the bulk screening rate ( $1/\tau_{sc}$ ) given by [29]:

$$R = \tau_{sc} / t_s \quad (1.2)$$

The switching time,  $t_s$ , encompasses the collective sum of domain growth and nucleation rates. Applied field magnitudes will determine which of these contributions will dominate; nucleation dominates at lower fields and growth dominates at higher fields [28]. An  $R$  value much less than 1 yields quasi-equilibrium conditions and there will be effective screening, an  $R$  equal to 1 yields off equilibrium conditions and there is incomplete screening, and an  $R$  much greater than 1 yields non-equilibrium conditions and ineffective screening [29]. The bulk screening process involves multiple contributions including moving bulk charges, reorienting defect dipoles, and injecting charge from the surface electrodes [29], [35]. These mechanisms work on time scales ranging from milliseconds to months, and so the microsecond switching times employed by some pulse poling studies would generate a large  $R$  constant and ineffective screening. More recent studies using wider pulse widths are likely outside of this  $R$  value threshold and thus do not exhibit

the fractal or dendritic domain microstructures characteristic of non-equilibrium screening conditions. This study will consider pulse poling samples using the non-equilibrium 10 $\mu$ s pulses. It will be argued that such conditions are pushing the system into a far-from-equilibrium state which allows for more isolated property enhancements than would otherwise not be expected from working in a near-equilibrium regime [36].

After a ferroelectric material has been poled, its properties tend to age slightly as the system relaxes to a more equilibrium state [37], [38], [39], [40]. Charges will begin to relocate and defect dipole associates will reorient as the domains partially re-randomize causing the overall properties to suffer [37], [41]. This process is most prevalent within the first few days after poling and will cause dielectric and piezoelectric coefficients to drop by roughly 1-5% [38]. Properties (for example, the  $d$  coefficient) will decrease according to the following stretched exponential relaxation [37]:

$$d = d_{\infty} + d_1 \exp[-(t/\tau)^{\nu}] \quad (1.3)$$

where  $d_{\infty}$  is the time independent contribution,  $d_1$  is a constant,  $t$  is time,  $\tau$  is the aging rate, and  $\nu$  is a constant between 0 and 1. This analytic function can be applied to a wider range of phenomenon and is sometimes referred to as the KWW theory, based on the works of Kohlrausch, Watson and Watt [42], [43]. As pointed out by Phillips, the  $\nu$  value often has physical meaning and describes whether the relaxation mechanisms at play result from long range interactions ( $\nu = 3/7$ ) or both long and short-range interactions ( $\nu = 3/5$ ) [44]. The reorienting defect dipoles within a system can be introduced on purpose, as seen in acceptor doping the system with Mn [45], [46]. Mn doping is often used to improve the temperature stability of a given material and boost its mechanical quality factor ( $Q_m$ ). This is accomplished by pinning domain wall motion through defect associated interactions between the acceptor site and oxygen vacancies [41], [46]. The objective of this study will be to test and model the aging behavior of Mn-doped relaxor materials (both single crystals and textured ceramics) subjected to HTPP. Most pulse poling studies apply pulses at room temperature, but this investigation chose to do it at elevated temperatures to improve domain wall mobility and increase the symmetry options near the so-called curved morphotropic phase boundary [47]. The properties of the given ferroelectric systems follow trends contrary to typical “negative” aging and show a more extreme aging behavior than earlier work into positively aging thin film piezoelectrics [48].

## 2. Experimental Procedure

### 2.1. Materials and Poling Conditions

Two Mn-doped relaxor systems were used for the majority of this study. The first was a 1 mol% Mn doped  $\text{Pb}(\text{In}_{1/2}\text{Nb}_{1/2})\text{O}_3\text{-Pb}(\text{Mg}_{1/3}\text{Nb}_{2/3})\text{O}_3\text{-PbTiO}_3$  (Mn: PIN-PMN-PT) single crystal (TRS Technologies, Inc., PA, USA) oriented in the [001] direction with dimensions of 5mm x 5mm x 0.5mm. The sample electrodes were sputtered on Au. The Mn-doped single crystals were DC

poled in an oil bath using a field of 7.5 kV/cm at 80°C for 15 minutes (Hipotronics, USA). For pulse poling, the crystals were subjected to 100 pulses with pulse widths of 10 μs and field strengths of 20 kV/cm at 80°C using a high voltage pulser (Instrument Research Company, USA). There was a wait time of 10 ms between each pulse for each material tested. Upon cooling back down to room temperature, a constant DC field of 10 kV/cm was applied to prevent domain back-switching. The second material was [001] textured 1 mol% Mn doped 0.4Pb(Mg<sub>1/3</sub>Nb<sub>2/3</sub>)O<sub>3</sub>-0.25PbZrO<sub>3</sub>-0.35PbTiO<sub>3</sub> (Mn: PMN-PZT) ceramic (Applied Research Lab, PA, USA) with dimensions of 22mm x 4mm x 2.4mm. These samples were electroded with fired on Ag paste and DC poled under a field of 25 kV/cm at 120°C for 15 minutes. For pulse poling, the textured samples were subjected to 100 pulses with pulse widths of 10 μs and field strengths of 20 kV/cm at 120°C with a DC field of 10 kV/cm during cooling down.

This study also tested a 1 mol% Sm doped Pb(In<sub>1/2</sub>Nb<sub>1/2</sub>)O<sub>3</sub>-Pb(Mg<sub>1/3</sub>Nb<sub>2/3</sub>)O<sub>3</sub>-PbTiO<sub>3</sub> (Sm: PIN-PMN-PT) single crystal (TRS Technologies, Inc., PA, USA) oriented in the [001] direction with dimensions of 5mm x 5mm x 0.5mm. This was done to show that the aging behavior detailed later in the paper is unique to Mn-doped materials possessing the associated Mn-oxygen vacancy defect dipoles. These samples were DC poled under a field of 7.5 kV/cm at 25°C for 15 minutes and pulse poled using 100 pulses with pulse widths of 10 μs and field strengths of 18 kV/cm at 120°C with a DC field of 9 kV/cm during cool down.

## 2.2. Electrical Characterization

Once the materials were poled, their dielectric and piezoelectric properties were measured and tracked with time to test how these samples aged. All measurement techniques were carried out following IEEE Standard 176-1987. The following baseline properties were measured immediately after poling then checked every 24 hours for the first week, every 48 hours for the next week, and finally on a weekly basis until properties appeared to stabilize. The piezoelectric coefficient ( $d_{33}$ ) was obtained using a combination of unipolar strain measurements and a Berlincourt meter (Piezo Meter, Piezotest, USA). The mechanical quality factor ( $Q_m$ ) and effective coupling coefficient ( $k_{eff}$ ) were measured using a precision impedance analyzer (4294A, Agilent Technology, USA). From the impedance data, these quantities were calculated with the following expressions [49]:

$$Q_m = \frac{f_r}{(f_1 - f_2)} \quad (2.1)$$

$$k_{eff} = \sqrt{1 - \left(\frac{f_r}{f_a}\right)^2} \quad (2.2)$$

where  $f_r$  is the resonance frequency,  $f_a$  is the antiresonance frequency, and the values of  $f_1$  and  $f_2$  represent the width of the impedance peak (using the 3dB method). The dielectric permittivity ( $\epsilon_{33}$ ) and  $\tan\delta$  of each sample were collected from an LCR meter measuring at 1 kHz (4140B, Hewlett Packard, USA).

In addition to tracking the basic piezoelectric and dielectric properties with time, the samples were also subjected to various measurements techniques before and after room temperature aging to discern the possible mechanisms at play. Among these were Rayleigh analysis wherein strain and polarization loops were collected by subjecting each sample to bipolar fields below their respective coercive fields [50], [51]. This was done using a Sawyer Tower circuit (609A, Trek Equipment, USA) in conjunction with a linear variable differential transducer (LVDT) [52]. This same system was used to collect hysteresis loops of samples before and after aging. Trends in permittivity and loss with temperature were obtained by heating the samples in a furnace (9023, Delta Design, USA) connected to an LCR meter which tracked capacitance and loss every 3°C. Using this same setup but instead measuring current every 3°C at a 3°C/minute heating rate, the pyroelectric current was measured. This data was then used to calculate changes in polarization with temperature using [53], [54]:

$$\Delta P = \frac{1}{A} \int \frac{I}{\beta} dT \quad (2.3)$$

where  $P$  is polarization,  $A$  is area,  $\beta$  is heating rate,  $I$  being the pyroelectric current, and  $T$  is temperature. X-ray diffraction (XRD) patterns were also collected during the aging process using a PANalytical Empyrean system (Malvern PANalytical, Great Britain). Finally, differential scanning calorimetry (DSC) (DSC2500, TA Instruments, USA) was performed on single crystal samples to track changes in latent heat signatures with aging.

### 3. Results and Discussion

#### 3.1. General Aging of Piezoelectric and Dielectric Properties

The aging trends for the DCP Mn-doped single crystal and textured ceramic samples are shown in Figure 2. All of the stretched exponential fittings included in Figure 2 follow Equation 1.3. The associated exponential terms and aging rates, together with errors for Figures 2 and 3, can be found in Table I. For both materials, the  $d_{33}$ , relative permittivity, and  $Q_m$  all decrease with time before stabilizing within a week after poling (though much of the aging is complete after a couple of days). This is to be expected from typical DCP ferroelectric materials as the system relaxes to a more favorable, less aligned configuration [37], [40], [55]. It is also evident that textured ceramics see a greater reduction in properties with time relative to single crystals. This is caused by the polycrystalline nature of these ceramics as grain-to-grain interactions lead to more complex aging mechanisms and space charges at the grain boundaries limit domain mobility [56], [57]. Despite this, textured ceramics do display less variability in properties, particularly in the case of dielectric permittivity. Reduced error in reported values can be attributed to the greater degree of compositional homogeneity found in textured ceramics [58], [59]. Bridgman grown crystals (like those employed by this study) tend to generate samples with some variability in composition from the same crystal boule [60]. Because of this phenomenon, sample to sample error in the single crystals is greater in Figures 2a-c relative to the textured ceramics in Figures 2d-f.

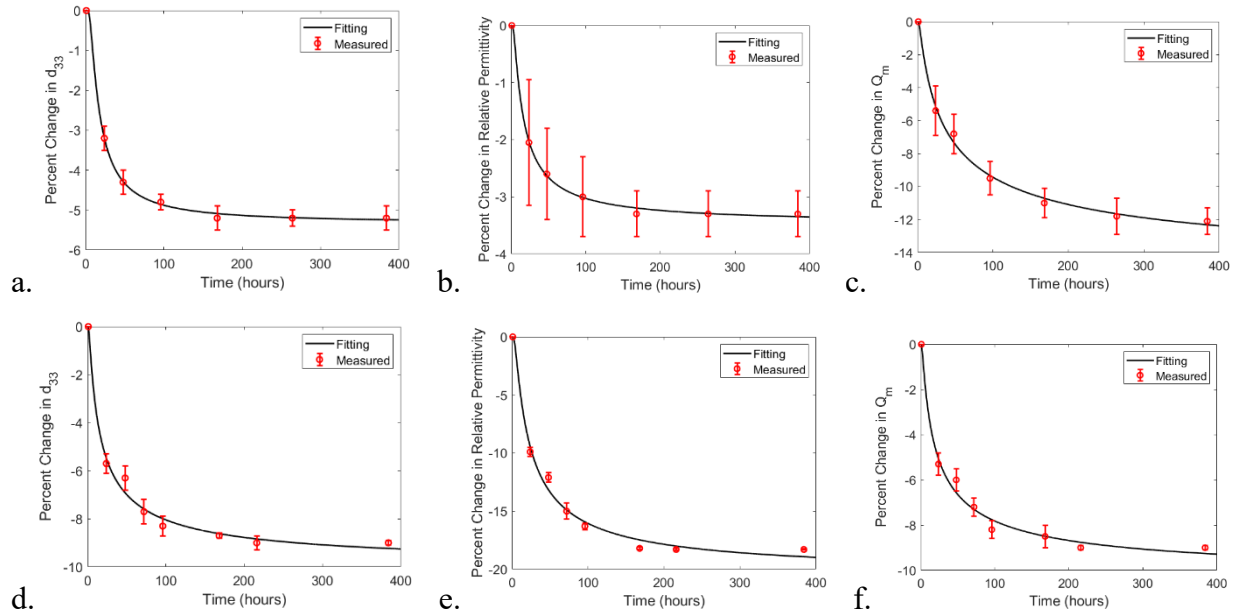


**Figure 2: DCP aging rates for (a)  $d_{33}$  of Mn: PIN-PMN-PT, (b)  $\epsilon_r$  of Mn: PIN-PMN-PT, (c)  $Q_m$  of Mn: PIN-PMN-PT, (d)  $d_{33}$  of Mn: PMN-PZT, (e)  $\epsilon_r$  of Mn: PMN-PZT, and (f)  $Q_m$  of Mn: PMN-PZT**

The results in Figure 2 are very different from those found in Figure 3. Dielectric and piezoelectric properties are observed to increase with time after HTPP. In addition, these samples saw their properties change to a larger degree than what is expected from DCP (40-60% in the case of crystals and 15-20% in the case of textured ceramics). Finally, the samples took longer to stabilize compared to DCP, with the crystals aging for up to a month and the textured ceramics aging for 2 weeks. The  $\tau$  values in Table I also give indirect evidence of the ability of pulse poling to decouple permittivity and piezoelectric response in these Mn-doped systems. The aging rates of  $d_{33}$  and  $\epsilon_r$  are comparable to each other for both systems following DCP while in the case of HTPP, the  $\tau$  of  $\epsilon_r$  is nearly double that of  $d_{33}$ . Other signs of this decoupling phenomenon have been reported in recent pulse poling efforts which saw large improvements in  $d_{33}$  relative to DCP while permittivity was relatively unchanged [Manuscript Submitted for Publication].

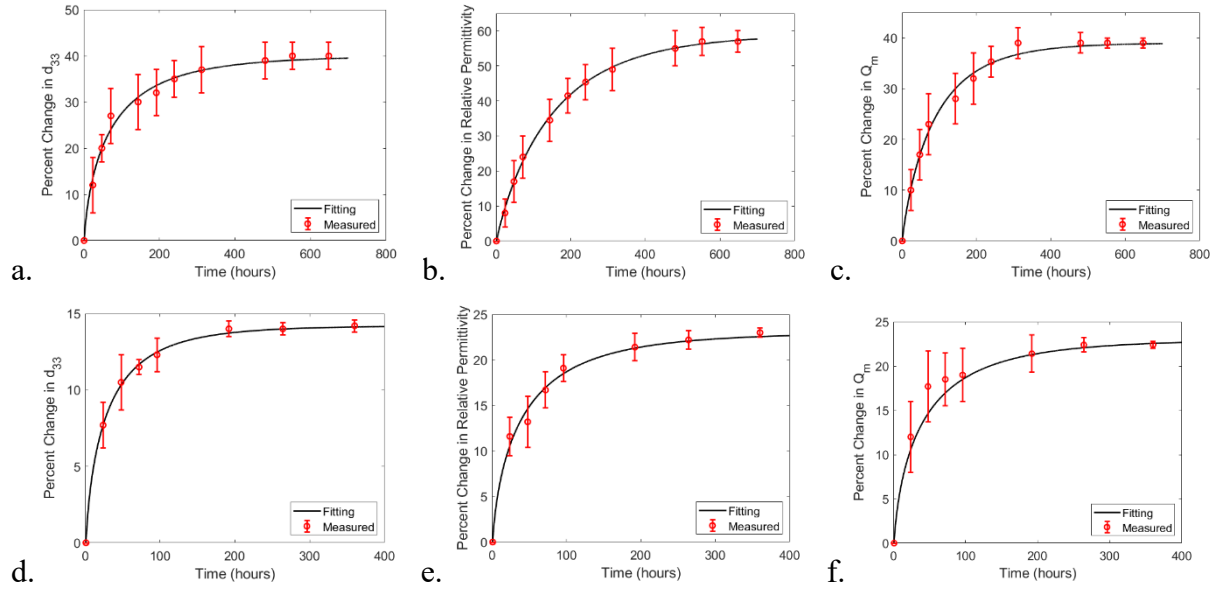


**Figure 3: HTPP aging rates for (a)  $d_{33}$  of Mn: PIN-PMN-PT, (b)  $\epsilon_r$  of Mn: PIN-PMN-PT, (c)  $Q_m$  of Mn: PIN-PMN-PT, (d)  $d_{33}$  of Mn: PMN-PZT, (e)  $\epsilon_r$  of Mn: PMN-PZT, and (f)  $Q_m$  of Mn: PMN-PZT**

**Table I: Aging Exponents ( $\nu$ ) and Time Constants ( $\tau$ )**

Material:	Poling Procedure:	Property of Interest:	$\nu$	$\tau$ (hours):
Mn: PIN-PMN-PT	DCP	$d_{33}$	$0.61 \pm 0.1$	$13.9 \pm 2.5$
Mn: PIN-PMN-PT	DCP	$\epsilon_r$	$0.47 \pm 0.05$	$12.5 \pm 3.8$
Mn: PIN-PMN-PT	DCP	$Q_m$	$0.55 \pm 0.11$	$29.3 \pm 9.2$
Mn: PIN-PMN-PT	HTPP	$d_{33}$	$0.66 \pm 0.10$	$73.7 \pm 9.0$
Mn: PIN-PMN-PT	HTPP	$\epsilon_r$	$0.72 \pm 0.11$	$144 \pm 2.5$
Mn: PIN-PMN-PT	HTPP	$Q_m$	$0.75 \pm 0.08$	$90.1 \pm 8.5$
Mn: PMN-PZT	DCP	$d_{33}$	$0.69 \pm 0.15$	$11.8 \pm 5.0$
Mn: PMN-PZT	DCP	$\epsilon_r$	$0.80 \pm 0.14$	$17.6 \pm 5.4$
Mn: PMN-PZT	DCP	$Q_m$	$0.64 \pm 0.09$	$14.6 \pm 6.4$
Mn: PMN-PZT	HTPP	$d_{33}$	$0.65 \pm 0.10$	$28.5 \pm 5.1$
Mn: PMN-PZT	HTPP	$\epsilon_r$	$0.64 \pm 0.15$	$41.8 \pm 6.0$
Mn: PMN-PZT	HTPP	$Q_m$	$0.65 \pm 0.11$	$42.1 \pm 3.1$

It is noted that “positive” aging has been reported occasionally in the past, though the scale of the increase in properties as well as the timelines involved are unique to HTPP. For example, a study into PZT thin films subjected to an ultraviolet (UV) imprint found that the  $d_{31}$  values of the films increased for the first  $10^5$  to  $10^6$  seconds after poling [48]. The increase in  $d_{31}$  was attributed to the existence of an excess field within the material which was slowly reduced over time to allow properties to recover. However, this aging phenomenon did not extend to the other properties of

the films, nor did it last as long as what is reported in Figures 3a-c. Previous researchers have also used a process known as de-aging to recover the properties of a material after poling has concluded [61], [62]. This once again does not explain the aging observed in HTPP given that de-aging requires the application of a bipolar field to induce an increase in properties over time. Positive aging occurs under ambient conditions, and thus a different mechanism to explain its origins will be offered in this study. It should be noted that this positive aging behavior was not seen in the HTPP Sm: PIN-PMN-PT crystal system (regarded as a soft piezoelectric composition) and it was unique to the hard Mn-doped materials studied here.

### 3.2. Evolution of Rayleigh Analysis Over Time

So, after observing positive aging in Mn-doped single crystals and textured ceramics, we must consider the origins underpinning this phenomenon. It is natural to first examine the two major contributions to piezoelectric properties: intrinsic or extrinsic. The intrinsic properties are equivalent to structural monodomain contributions and extrinsic properties are derived from domain and phase boundary motion under applied electric fields [63]. The Rayleigh analysis is a powerful technique used to separate the extrinsic/irreversible contributions to the dielectric and piezoelectric coefficients from the intrinsic/reversible contributions [50], [51]. It was therefore performed on both Mn-doped systems poled via HTPP before and after the aging process. Upon the application of a series of bipolar fields below 50% of the coercive field of a given material, the dielectric and piezoelectric responses can be characterized in the following way [64]:

$$d = d_{\text{init}} + \alpha E_0 \quad (3.1)$$

$$\varepsilon = \varepsilon_{\text{init}} + \alpha E_0 \quad (3.2)$$

where  $d$  and  $\varepsilon$  are the measured piezoelectric and dielectric coefficients respectively,  $d_{\text{init}}$  and  $\varepsilon_{\text{init}}$  encompass the intrinsic response and reversible domain wall motion,  $E_0$  is the amplitude of the applied electric field, and  $\alpha$  is the Rayleigh coefficient. When plotting applied electric field vs. the measured  $d_{33}$  or  $\varepsilon_{33}$ , the slope of the linear region of the plot represents the extrinsic/irreversible contributions while the y-intercept corresponds to the intrinsic/reversible contributions [50]. The Rayleigh plots for these two materials before and after aging are shown in Figure 4.

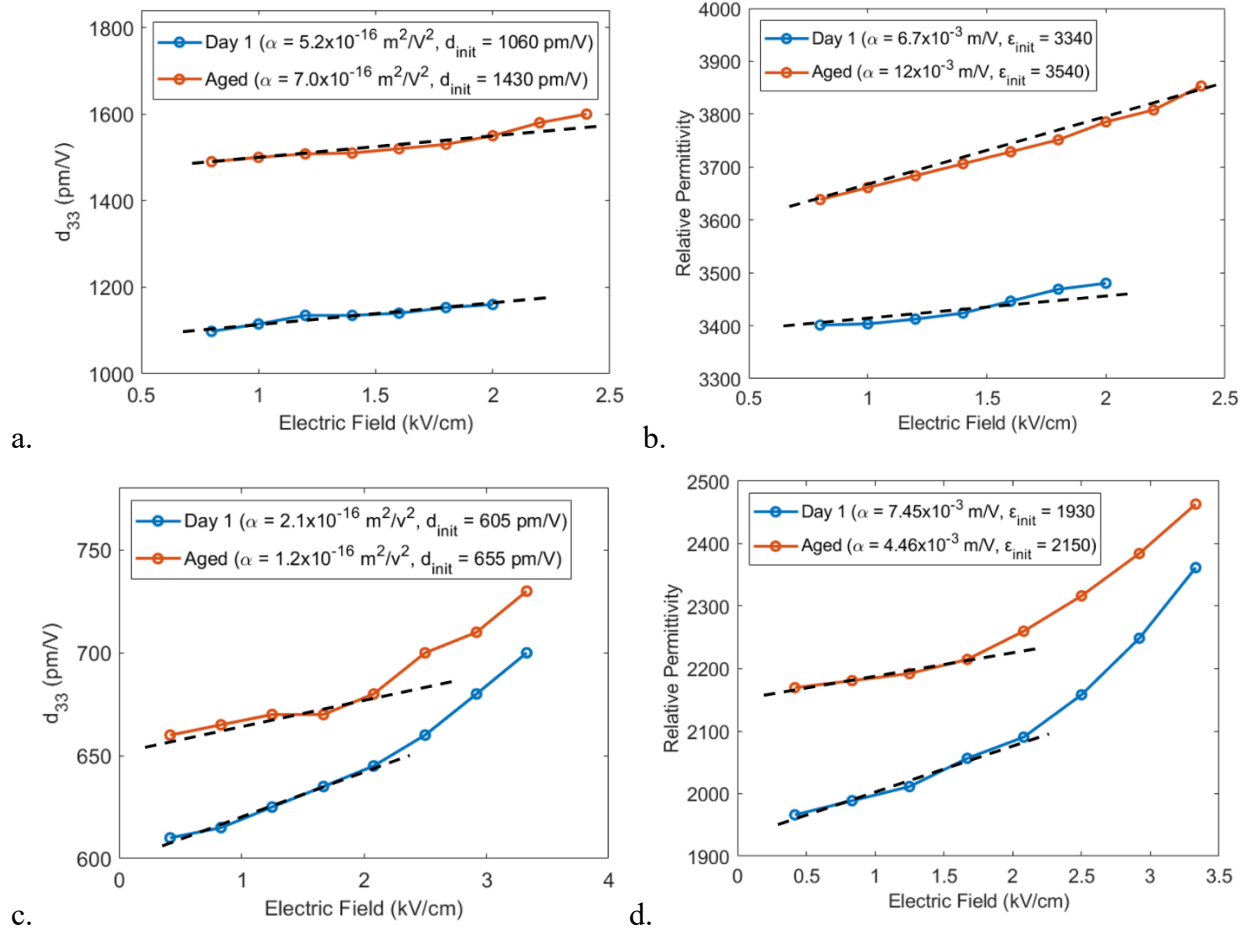


**Figure 4: HTPP Rayleigh plots showing (a)  $d_{33}$  vs.  $E$  for Mn: PIN-PMN-PT, (b)  $\epsilon_{33}$  vs.  $E$  for Mn: PIN-PMN-PT, (c)  $d_{33}$  vs.  $E$  for Mn: PMN-PZT, and (d)  $\epsilon_{33}$  vs.  $E$  for Mn: PMN-PZT**

From Figure 4a-b, it is evident that the single crystal system experiences a slight increase in  $\alpha$  with time. This would suggest that the mobility of non- $180^\circ$  domain walls is increasing or the number of pinning sites in the material is decreasing [51]. However, there is an opposite trend observed for textured materials. As shown in Figure 4c-d,  $\alpha$  decreases with time for the textured ceramics. While there is no clear consensus on these two systems based on this data when it comes to extrinsic or irreversible contributions, there is a consistent trend when it comes to the aging of intrinsic/reversible contributions. Both the single crystal and textured ceramic materials saw their y-intercepts increase with time corresponding to a change in intrinsic or irreversible character. It can further be hypothesized that if both materials exhibit positive aging, but only the intrinsic or reversible characteristics age in similar ways, positive aging is likely dominated by a change in the intrinsic nature of the ferroelectric poled state or reversible domain wall motion.

### 3.3. Structural Considerations

Figure 5 shows how trends in permittivity and loss with temperature changed for the two systems upon aging following HTPP. Immediately after poling, the materials appear to show no

peaks in permittivity or loss where the rhombohedral to tetragonal transition temperature ( $T_{rt}$ ) is typically located. With time, the dielectric anomaly then appeared and the permittivity values at room temperature increased according to the rates quantified in Figure 3. The suppression of this peak is not currently well known; however, it does suggest that the system may be placed into a metastable structural state on day one that relaxes with time [65]. Compositional inhomogeneities within Bridgman grown crystals can lead to fluctuations in  $T_{rt}$  as the  $PbTiO_3$  content varies along the length of PMN-PT based boules [66]. The Mn: PIN-PMN-PT samples used in this study were no different, and samples possessed a range of  $T_{rt}$  values. It was found that occasionally not all the Mn-doped single crystal samples exhibited positive aging, and only those with  $T_{rt}$  values close to the pulse poling temperature ( $80^\circ\text{C}$ ) aged in this manner. This points to the aging behavior's reliance on pulsing the system near a non-equilibrium and transitory state with likely more symmetry options available. In this disordered configuration, the system is easily pushed to a far from equilibrium state as the material threads the quickest path to accommodate such swift pulses of electric field. The textured Mn: PMN-PZT samples possessed greater compositional homogeneity (yielding consistent  $T_{rt}$  values) and demonstrated positive aging 100% of the time.

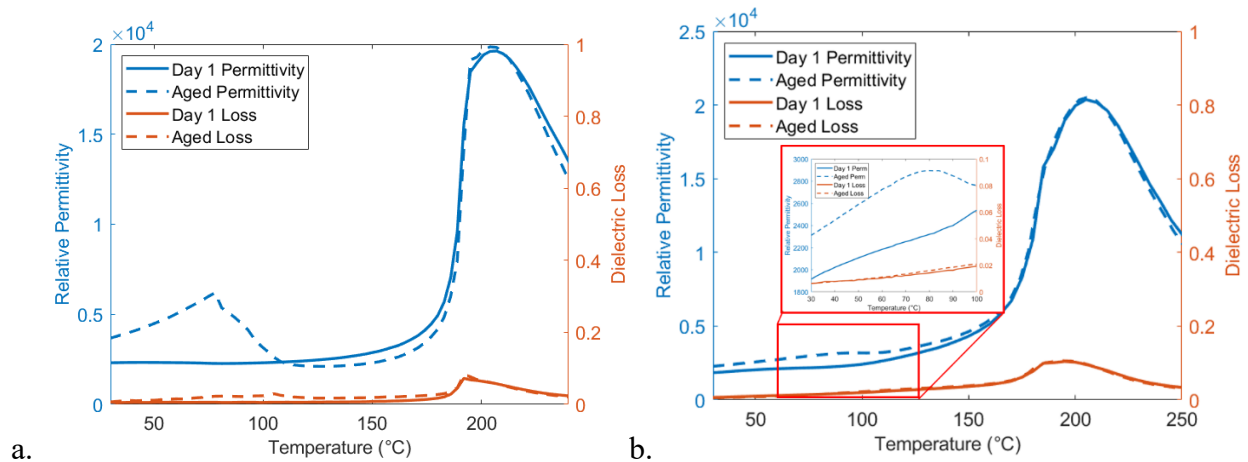


**Figure 5: Permittivity and dielectric loss at 1 kHz as a function of temperature for (a) Mn: PIN-PMN-PT and (b) Mn: PMN-PZT**

The dielectric anomaly in Figure 5a for the Mn: PIN-PMN-PT system appears to show 2 peaks in and around  $T_{rt}$ . Previous studies into alternating current poling (ACP) single crystals have also reported a double peak anomaly forming after poling [67], [68]. It has been speculated that such a two peak feature is associated with the existence of a monoclinic phase in materials possessing compositions near the morphotropic phase boundary [67]. The existence of this monoclinic phase could also explain the improved properties that are possible in piezoelectrics that have been poled using ACP [69]. In the context of HTPP, this line of reasoning would follow the increase in properties that are observed before and after the performance-enhancing monoclinic phase appears in the single crystals. Traces of monoclinic ferroelectric phases altering the typical rhombohedral lattice also support the argument that positive aging is driven by an intrinsic change

in the system as was hinted towards within the Rayleigh data. Although at this time the crystallographic nature of the HTPP ferroelectric state has not been comprehensively investigated, it is conceivable that symmetries lower than monoclinic are also a possibility as has been hypothesized by Vanderbilt et al. [70]

The case for the monoclinic ferroelectric phase forming overtime is further strengthened by the XRD pattern evidence in Figure 6. From day one to aged, the Mn: PIN-PMN-PT system sees its (100) and (200) diffraction peaks broaden and shift to higher 2-theta values. Such behavior corresponds to a shortening of the 3-axis (poling direction) and is consistent with the introduction of a monoclinic phase to the material, as reported earlier [68]. Much of the shifting happens within the first 48 hours, which matches the stretched exponential nature of the aging mechanism [37], [44]. From both the changes in permittivity behavior as well as the XRD data, positive aging appears to have a large dependence on structural alterations and phase transitions. These lattice distortion trends would be more consistent with intrinsic properties rather than domain dynamic extrinsic contributions in HTPP samples under the positive aging process.

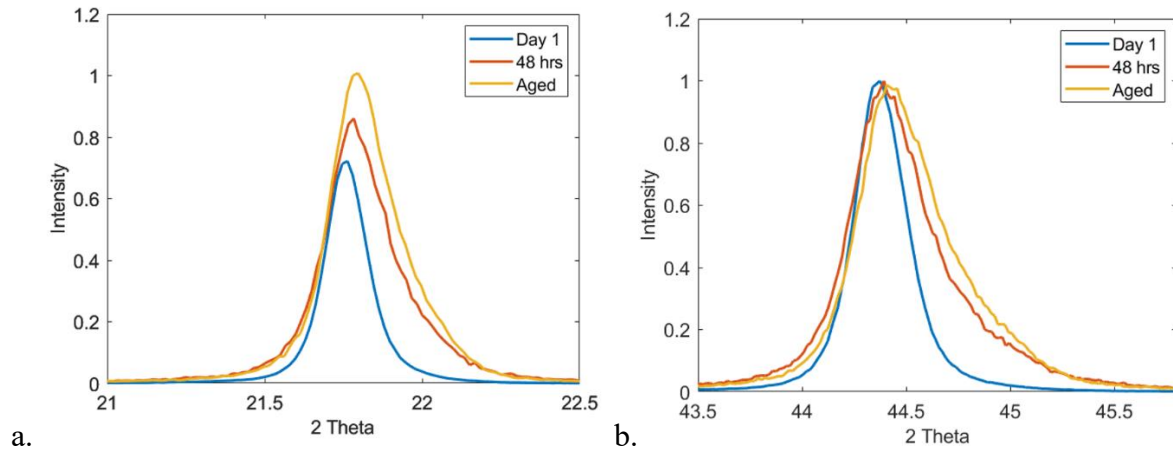


**Figure 6: Aging of the (100) and (200) pseudo cubic perovskite peaks in the XRD pattern for Mn: PIN-PMN-PT after HTPP.**

### 3.4. Pyroelectric Behavior

A typical pyroelectric current plot for a DCP relaxor material is shown in Figure 7a, which was then used to quantify the polarization with temperature plot in Figure 7b according to Equation 2.3. The peaks in Figure 7a are depolarization events, and previous work into DCP pyroelectric responses links the initial peak to the rhombohedral to tetragonal phase transition [71]. These events correspond to gradual decays in  $P_r$  as shown in Figure 7b, which is consistent with normal relaxor behavior [72]. The final current peak in Figure 7a is associated with the depolarization temperature ( $T_d$ ) which for relaxors will be below  $T_c$  [3]. Figures 7c-d show a different behavior for the HTPP Mn: PIN-PMN-PT system. Rather than exhibiting gradual decays in  $P_r$ , the polarization plots in Figure 7d for the aged and unaged crystals feature sharp decreases in polarization at the Curie temperature,  $T_c$ . This indicates that the system is now acting more like a

normal ferroelectric and has largely lost its relaxor diffuse transition characteristics following HTPP [5], [23]. The implications of such a shift in behavior are further discussed in Section 3.5.

It is also worth noting that before aging, there is no current peak in Figure 7c where the  $T_{rt}$  should typically be. This is like the observation in the permittivity results as discussed in Figure 5a which showed no signs of a transition at this temperature. With time, the aging relaxation process occurs and a peak in pyroelectric current does appear, though it is in the opposite direction to the primary pyroelectric current. This will thus counteract the expected reduction in polarization with increasing temperature as the material approaches  $T_{rt}$ . Previous pyroelectric studies have stated that the existence of a negative current indicates an internal electric field,  $E_{int}$ , in the poling direction [73], [74]. This would suggest that an internal field of  $E_{int}(t)$  is developing over time, the formation of which coincides with increases in dielectric and piezoelectric properties. Evidence of a finite internal electric field is further seen in the shift in  $T_c$  observed after aging. It has been well documented that the application of an electric field in the poling direction during pyroelectric measurements will push  $T_c$  to higher values and preserve polarization for higher temperatures on heating [74], [75]. One study by Kim et al. observed negative pyroelectric currents in their Mn: PMNT system following the so-called “self-poling” process [71]. They concluded that such currents arose due to an internal electric field from the alignment of  $Mn^{2+} - V_O$  defect dipoles. This reasoning is consistent with the proposed explanation of the currents in Figure 7c as well as positive aging as a whole given that these phenomena are only observed in systems that feature Mn doping. It is therefore anticipated that defect dipoles within the system are randomized during HTPP and then reorientate during aging, forming a time dependent internal field that is minimizing an uncompensated depolarization field. This process is also aided by a decrease in room temperature polarization and an increase in relative permittivity, in accordance with Equation 1.1.

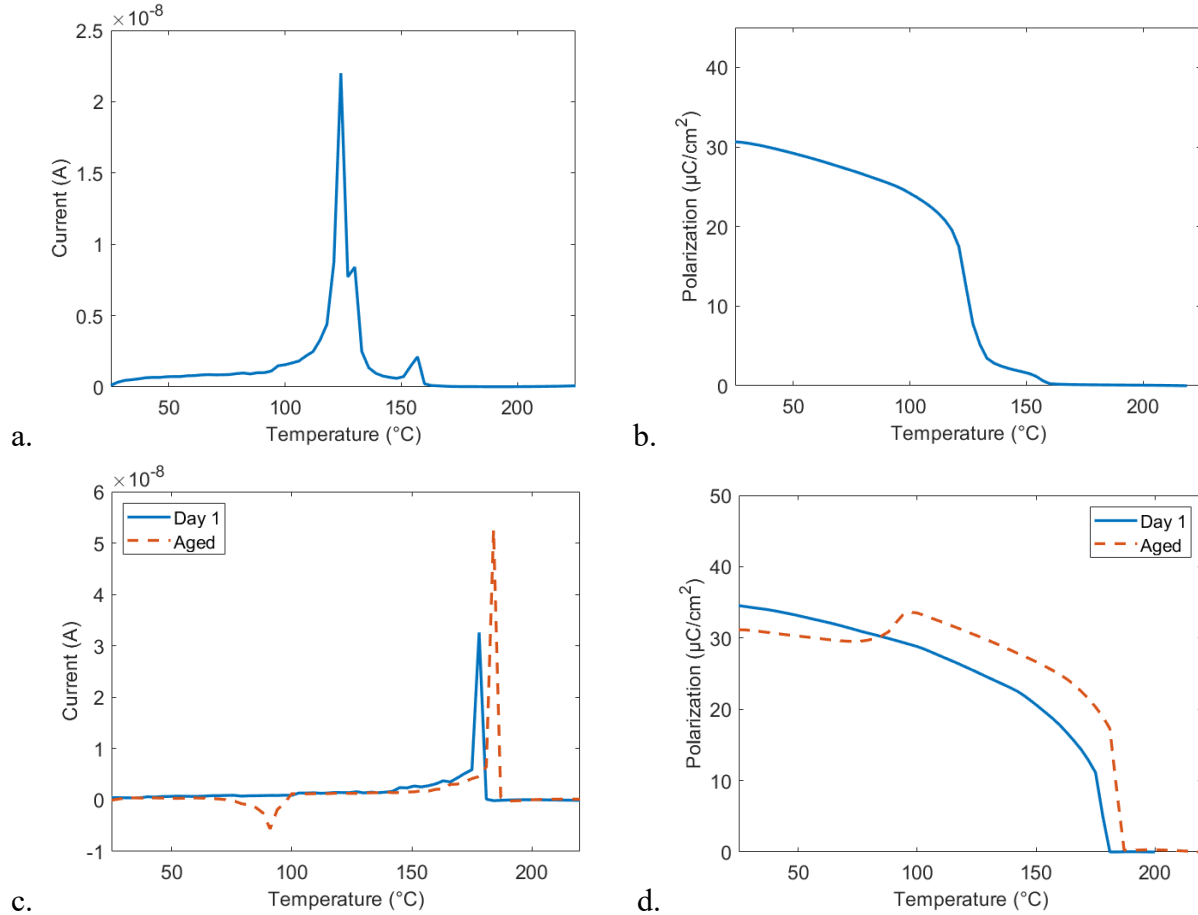


**Figure 7: Plots showing temperature dependence of (a) pyroelectric current for DCP Mn: PIN-PMN-PT, (b) polarization for DCP Mn: PIN-PMN-PT, (c) pyroelectric current for HTPP Mn: PIN-PMN-PT, and (d) polarization for HTPP Mn: PIN-PMN-PT.**

So, qualitatively, we have noted there is a lot of variation under positive aging relaxation in terms of property changes and the appearance/shifting of phase transitions. The most likely and self-consistent understanding of this is that the pulse poling conditions used here enable the system to be driven to a far from equilibrium state. This state contains an uncompensated depolarization field, and the system adjusts to rectify this unstable state, including the development of an internal field.

### 3.5. Application of Landau-Devonshire Theory

The Rayleigh analysis previously showed that after HTPP, the aging of strain and polarization field dependencies is mostly the result of an intrinsic or reversible domain wall contribution. Evidence for an intrinsically dominated change can be found in comparing Figure 7b to Figure 7d. It appears that HTPP is changing the order of the paraelectric to ferroelectric phase transition at  $T_c$ . As opposed to the diffuse decrease in polarization expected from a relaxor material in Figure 7b, there is a sharp decrease in polarization following HTPP in Figure 7d which is more in line with normal ferroelectrics [12], [75], [76]. This behavior can be classified qualitatively as

a weak first order phase transition which allows for the application of the Landau-Devonshire Theory (which will colloquially be referred to as the Landau Theory from here on) [77], [78]. Landau Theory provides a phenomenological pathway to explain changes in ferroelectric phase transitions and properties for materials exhibiting first, tri-critical, or second order phase transitions [79]. It can be described thermodynamically with the following equation [79]:

$$F(T, P) = F_o(T) + \frac{1}{2}\alpha P^2 + \frac{1}{4}\beta P^4 + \frac{1}{6}\gamma P^6 \quad (3.3)$$

where  $F$  is the Helmholtz free energy,  $T$  is temperature,  $P$  is polarization, and  $\alpha$ ,  $\beta$ , and  $\gamma$  are the principal coefficients. Within Landau Theory,  $\alpha$  is temperature dependent while  $\beta$  and  $\gamma$  are temperature independent. The sign of the  $\beta$  quartic term will also dictate the order of the phase transition, with a negative  $\beta$  indicating first order, a positive  $\beta$  indicating second order, and a  $\beta$  of 0 representing the tri-critical phase transition [79]. Landau Theory was applied to the HTPP system in order to verify the change in reaction order taking place and better explain the positive aging trends observed. We also note that typically, the idea of applying a Landau model to a relaxor material is not a route we would advise. However, as will be seen below, under this far from equilibrium state it will be applicable.

Taking electrostrictive coupling considerations into account requires the use of the elastic Gibbs free energy of the system. The full derivation of this expression from the Helmholtz free energy with strain-polarization coupling is provided in the supplemental section, but the result is given by [80]:

$$G(T, X, P) = \frac{1}{2}\left(\alpha + \frac{Q}{c}X\right)P^2 + \frac{1}{4}\left(\beta - \frac{Q^2}{2c}\right)P^4 + \frac{1}{6}\gamma P^6 - \frac{X^2}{2c} \quad (3.4)$$

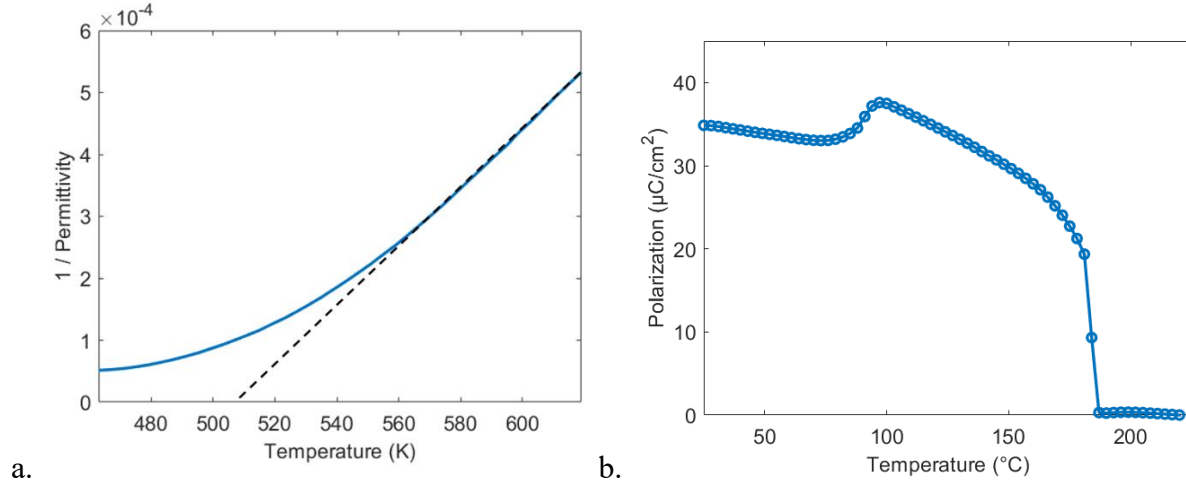
where  $Q$  is the electrostrictive coefficient,  $x$  is strain,  $X$  is stress, and  $c$  is the stiffness of the material. Under zero stress conditions, these electrostrictive considerations become nullified except for the all-important quartic  $\beta$  term. Thus, it would be anticipated that any aging observed in  $Q$  or  $c$  could impact the first or second order nature of the  $T_c$  transition as well as the discontinuous onset of polarization.

Figure 8a shows the inverse of permittivity as a function of temperature which can be used to derive the Curie constant ( $C$ ) and a temperature independent term represented by  $\alpha_o$  [12]. These quantities are calculated according to the following equations [75], [79]:

$$C = \frac{dT}{d(1/\epsilon)} \quad (3.5)$$

$$\alpha_o = \frac{1}{\epsilon_o C} \quad (3.6)$$

So,  $C$  is the inverse of the slope of the linear region in Figure 8a which was found to be  $2.09 \times 10^5$  K. Using this value,  $\alpha_o$  was calculated as  $5.42 \times 10^5 \text{ mF}^{-1}\text{K}^{-1}$ . In Figure 8b, the final value of polarization before it drops to 0 at  $T_c$  is denoted as  $P_o$  which for this system was  $11 \mu\text{C}/\text{cm}^2$ .



**Figure 8: Plots showing temperature dependence of (a) 1/Permittivity for aged HTPP Mn: PIN-PMN-PT and (b) polarization for aged HTPP Mn: PIN-PMN-PT**

While the sharp decrease in polarization in Figure 8b is a strong argument for the transition becoming first order, a difference in the heat flow at this point would serve as more definitive proof. Also, the data from the measured latent heat peak is helpful in deriving the rest of the Landau coefficients. Figure 9 shows the results of measuring the heat flow of DCP and HTPP Mn: PIN-PMN-PT samples using differential scanning calorimetry (DSC). There is a drastic difference between the heat signatures recorded for these two poling methods. The DCP sample displays an expected muted peak at  $T_c$  while the HTPP sample features a more significant anomaly. In fact, the normalized peak height for the HTPP sample is 17 times larger than that of the DCP. The existence of a strong latent heat peak is indicative of a first order phase transition [81]. Such a drastic shift in behavior at this transition once more points to a change in the intrinsic properties of the material. One would not expect differences in domain dynamics (in both reversible and irreversible motion) to account for a significant change in the latent heat of a material. Pulse poling at elevated temperatures pushes the material into a far-from-equilibrium state which allows for changes to the basic characteristics of the system. The path that the material is taking to relax back down from this metastable state is driving the material in a new intrinsic regime contrary to its expected relaxor designation. This initial non-equilibrium regime is attainable due to the exceedingly fast switching rates employed by pulse poling coupled with the disordered state of the material when poling near transition temperatures.

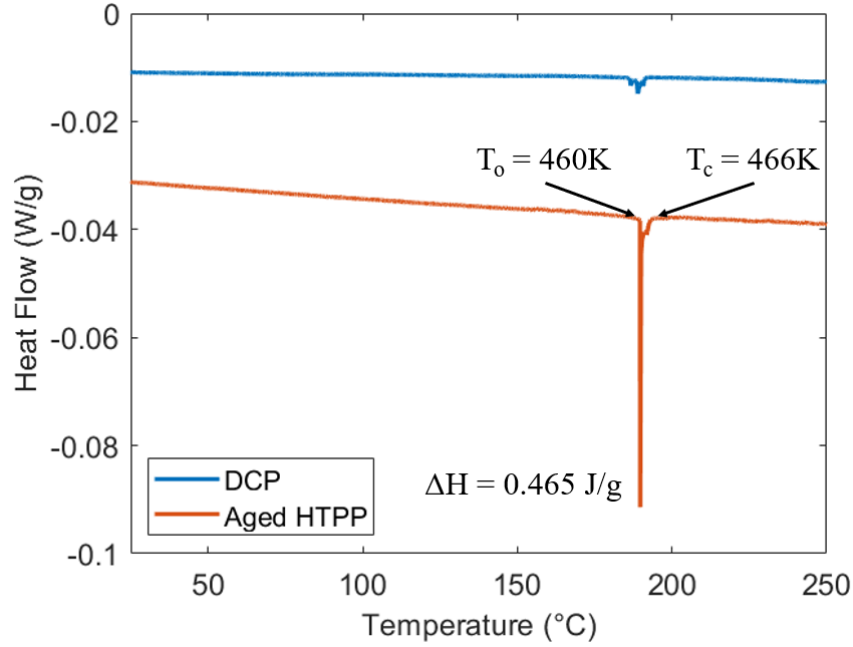


**Figure 9: Heat flow as a function of temperature for Mn: PIN-PMN-PT**

Turning now to the remaining Landau coefficients, the change in enthalpy,  $H$ , associated with the phase transition in Figure 9 can be used to calculate these unknowns via the following equations [75], [79]:

$$\frac{\Delta H}{T_c} = \frac{1}{2} \alpha_o P_o^2 \quad (3.7)$$

$$P_o^2 = -\frac{3\beta}{4\gamma} \quad (3.8)$$

$$T_c - T_o = \frac{3\beta^2}{16\alpha_o\gamma} \quad (3.9)$$

Using these equations, the various Landau coefficients were all calculated, and these are included in Table II along with the coefficients of other first order ferroelectric systems. The coefficients derived in this study are within the range of expected values for perovskite based ferroelectric materials with first order properties within the framework of the Landau Theory. Also, it is worth noting that the experimental data yielded a negative  $\beta$  value. This indicates that the material is undergoing a first-order phase transition which again is contrary to typical relaxor ferroelectrics [77], [81].

**Table II: Landau Coefficients Comparison**

Material:	$\alpha$ (m/F):	$\gamma$ (Vm <sup>9</sup> C <sup>-5</sup> )	$\beta$ (Vm <sup>5</sup> C <sup>3</sup> )
Mn: PIN-PMN-PT (This Paper)	$3.25 \times 10^6$	$6.53 \times 10^{10}$	$-1.06 \times 10^9$
BaTiO <sub>3</sub> [79]	$8.1 \times 10^6$	$2.2 \times 10^{10}$	$-9.6 \times 10^8$
BaTiO <sub>3</sub> [82]	$9.0 \times 10^6$	$1.6 \times 10^{10}$	$-5.2 \times 10^8$
PbTiO <sub>3</sub> [83]	$6.66 \times 10^5$	$2.7 \times 10^{11}$	$-3.56 \times 10^9$

There have also been studies investigating the impact of an internal electric field on phase transitions in the context of Landau Theory [75]. The same latent heat peak data in Figure 9 can help to find the magnitude of an internal field at  $T_c$  according to the following equation [75]:

$$\Delta T_c = \frac{E\Delta P}{\Delta S} \quad (3.10)$$

where  $\Delta T_c$  is the shift in Curie temperature first discussed in Figure 7d,  $E$  is the magnitude of the internal electric field,  $\Delta P$  is the change in polarization during the phase transition, and  $\Delta S$  is the change in entropy calculated from the measured  $\Delta H$  value. With this, the internal field was found to be 2.69 kV/cm at  $T_c$ . This value exceeds previously reported internal field values in “self-poling” Mn: PMNT which researchers claimed could facilitate a restoration of piezoelectric properties after depoling [71].

The impact that electrostrictive coupling has on the aging process is clear in the impedance responses in Figure 12. Upon aging, the resonance frequency of the Mn: PIN-PMN-PT and Mn: PMN-PZT systems decreased by 18% and 3% respectively. This decrease relates to a decrease in elastic stiffness as shown by the following [49]:

$$f_r = \frac{1}{2l} \sqrt{\frac{c}{\rho}} \quad (3.11)$$

where  $f_r$  is the resonance frequency,  $l$  is sample thickness,  $c$  is the elastic stiffness, and  $\rho$  is density. The values of  $Q$  and  $c$  pre and post aging are given in Table III. The electrostrictive coefficient,  $Q$ , was determined using a strain vs.  $P^2$  plot, an example of which is given in the supplemental section. So, relating this back to Equation 3.4, a more compliant matrix makes the  $\beta$  coefficient more negative which in turn makes the phase transition more first order with aging. For comparison, DCP data is also included in Table III and it should be noted that  $Q$  and  $c$  did not notably change with DCP negative aging.

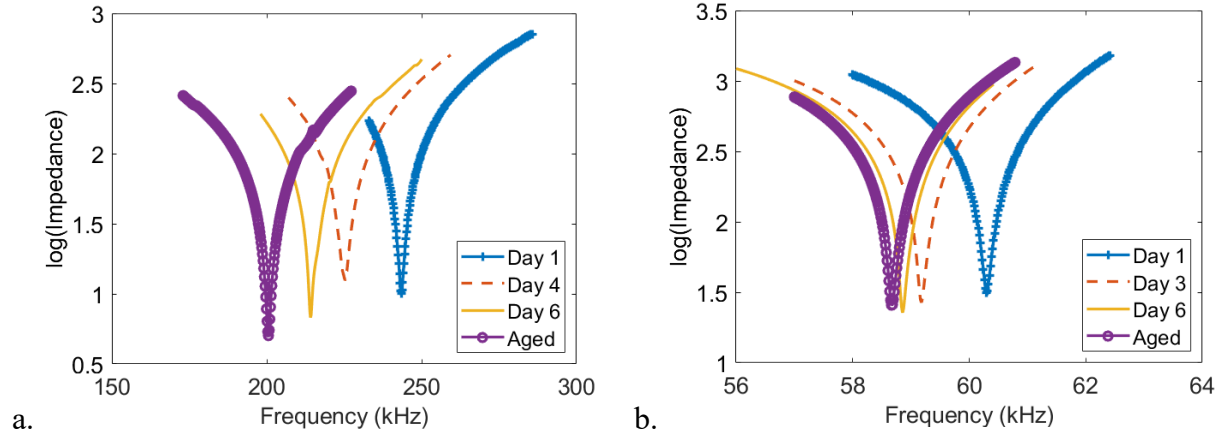


**Figure 10: Shift in resonance frequency with aging for (a) HTPP Mn: PIN-PMN-PT and (b) HTPP Mn: PMN-PZT**

**Table III: Values of Q and c for DCP and HTPP**

Material:	Poling:	Q ( $m^4C^{-2}$ ):	c ( $Nm^{-2}$ ):
Mn: PIN-PMN-PT	DCP	$6.07 \times 10^{-2}$	$4.17 \times 10^8$
Mn: PIN-PMN-PT	HTPP (Day 1)	$6.00 \times 10^{-2}$	$4.81 \times 10^8$
Mn: PIN-PMN-PT	HTPP (Aged)	$6.32 \times 10^{-2}$	$3.27 \times 10^8$
Mn: PMN-PZT	DCP	$9.95 \times 10^{-2}$	$6.60 \times 10^8$
Mn: PMN-PZT	HTPP (Day 1)	$8.64 \times 10^{-2}$	$6.80 \times 10^8$
Mn: PMN-PZT	HTPP (Aged)	$13.3 \times 10^{-2}$	$6.43 \times 10^8$

The Landau theory confirms the qualitative property inferences that we suspected and shows that HTPP gives a non-equilibrium state that is first order in nature. These first order characteristics appear to increase with aging alongside increases in general properties. Electrostrictive coupling accounts for the trends in the time dependence of first order behavior; largely being the result of a time reduction in elastic stiffness, c, and increase in the electrostrictive coefficient, Q.

### 3.6. Internal Field Implications

With the properties now well described by the intrinsic Landau theory, their understanding can be further expanded with respect to phenomenological models by determining the time dependence of the internal field under the positive aging process. To confirm the existence of an internal field developing in the material, hysteresis loops were collected before and after aging and are included in Figure 10. It is evident in both systems that there is a major shift in the shape of the hysteresis loop with time as the aged samples show a highly asymmetric leftward bias. This confirms that the internal field is not present on day one and is created during the positive aging process (and very likely is a key driver of that process). To quantify the magnitude of this internal

field, the following equation was used and the resulting values for several samples can be found in Table IV [84]:

$$E_{int} = \frac{E_c(1) + E_c(2)}{2} \quad (3.10)$$

where  $E_{int}$  is the internal electric field and  $E_c(1)$  and  $E_c(2)$  are the measured coercive field values.

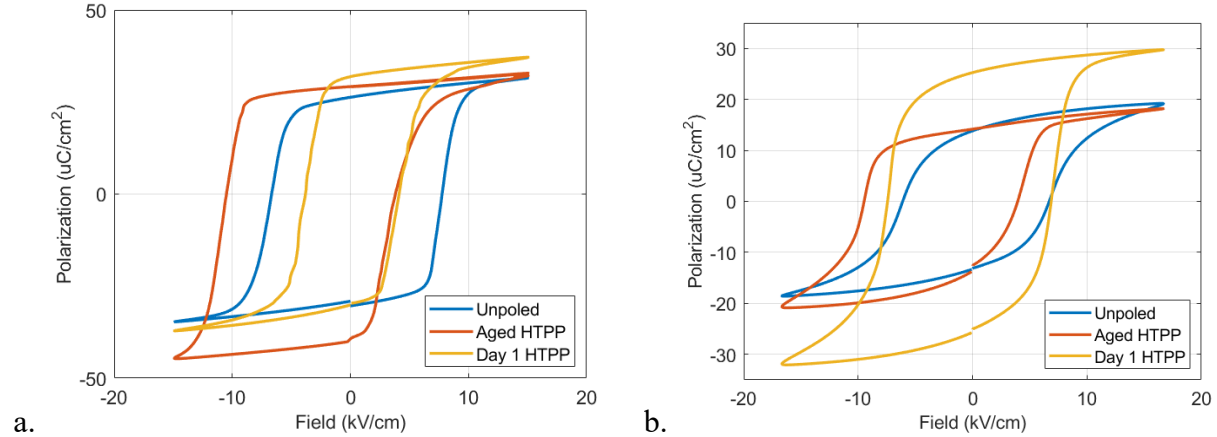


**Figure 10: Hysteresis loops for (a) Mn: PIN-PMN-PT and (b) Mn: PMN-PZT**

**Table IV: Measured  $E_{int}$  values**

Material	Poling Method:	$E_c(1)$ , (kV/cm):	$E_c(2)$ , (kV/cm):	$E_{int}$ (kV/cm):
Crystal	Unpoled	7.1	6.15	0.20
Crystal	DCP	4.15	3.35	0.40
Crystal	HTPP (day 1)	4.10	3.70	0.20
Crystal	HTPP (aged)	3.65	10.6	3.48
Textured	Unpoled	6.74	6.09	0.32
Textured	DCP	5.76	8.25	1.24
Textured	HTPP (day 1)	7.43	6.90	0.27
Textured	HTPP (aged)	3.97	9.47	2.75

From the results in Table IV, these systems do inherently possess some asymmetry with respect to the electric field axis; this is to be expected from materials with defect dipoles that arrange in preferential directions [84], [85]. However, the aged HTPP samples still demonstrate a significantly higher internal field that is absent on day one. The formation of this field under relaxation is likely due to the alignment of defect dipoles which again explains why this aging behavior was only seen in the Mn-doped materials. After being dissociated and/or randomized during the pulse poling process, the  $Mn^{2+}$  ions and mobile oxygen vacancies rotate in the direction of  $P_r$  leading to a shift in the hysteresis loop with time [41], [86]. Such phenomena have been documented in the past with Mn-doped single crystals, and these studies also report that the  $P_r$  of

the material will decrease with aging due to space charge accumulation [85], [86]. The aged HTPP samples exhibited this same decrease in  $P_r$  as shown in Figure 10. The measured internal field of the single crystal at room temperature (3.48 kV/cm) is also less than that calculated at  $T_c$  using the Landau Theory (2.69 kV/cm). Defect dipoles are again the culprit as higher temperatures cause these dipoles to become decoupled and dissociated, leading to a decrease in the formed  $E_{int}$  [85]. There is therefore a temperature dependence on the internal field in the aged samples.

The following phenomenologically derived expression reveals the impact that an internal electric field could be expected to have on the effective piezoelectric coefficient based on strain data. Its derivation can be found in the supplemental section.

$$d_{eff} = \frac{dx}{dE} = 2ME_{int} + 2Q\epsilon_r\epsilon_0P_s \quad (3.11)$$

where  $M$  is related to the electrostrictive coefficient  $Q$  via  $M = Q\epsilon_o^2\epsilon_r^2$ . So, at the beginning of the aging relaxation there is negligible internal field causing the first term to go to zero. The measured  $d_{33}$  should thus match the intrinsic expression in Equation 3.11. Indeed, this turns out to be the case for the Mn: PIN-PMN-PT system as the theoretical  $d_{33}$  of  $998 \pm 55$  pC/N matches the average measured value of  $990 \pm 40$  pC/N. Then, as the internal field begins to form, the measured value should now take the entirety of Equation 3.11 into consideration. Again, there is self-consistency in the results as an  $E_{int}$  of 3.48 kV/cm generates a theoretical value of  $1,422 \pm 65$  pC/N which closely matches the experimental value of  $1,435 \pm 55$  pC/N for room temperature performance. A similar agreement was found in the textured hard piezoelectric ceramics.

While common defect dipole alignment can explain the formation of the internal field, relating its creation to the not-so-common positive aging requires once more viewing HTPP from a far-from-equilibrium perspective. When pulse poling a material at an elevated temperature, two phenomena occur simultaneously. The first is the ineffective screening of the depolarization field that arises due to the exceedingly fast switching rates and correspondingly high R coefficient [29]. Under these non-equilibrium conditions, bulk screening mechanisms (such as defect dipole realignment) cannot move fast enough and an excess depolarization field opposite the poling direction is left in the material. The second phenomenon is the complete dissociation and misalignment of the defect dipoles that comes from pulsing at a high-entropy state such as the  $T_{rt}$  transition. As the system attempts to respond to the swift poling procedure, new accommodation pathways become available as the material is highly unstable. Thus, the material is thrust into an intrinsically different state far from its typical equilibrium position. Given the fact that the alignment direction of the defect dipoles is dependent on the crystal symmetry of the host lattice, changes to said lattice would clearly impact these dipoles [87]. HTPP has shown signs of introducing a monoclinic phase into the system which would possess 12 (or more) potential polarization directions, higher than the 6 found in tetragonal or the 8 found in rhombohedral [70]. Thus, there exist more ways in which to align the defect dipoles, making their collective orientation more disordered than usual. With time, the unaccommodated depolarization field must be compensated, and an internal field is generated by the realigning defect dipoles. As the defect

dipoles align in the poling direction, their generated  $E_{int}$  counteracts the residual excess  $E_{rd}$ . The suppressive effect that a runaway  $E_{rd}$  would have on properties is thus slowly removed resulting in positive aging. A schematic detailing this process is shown in Figure 11.

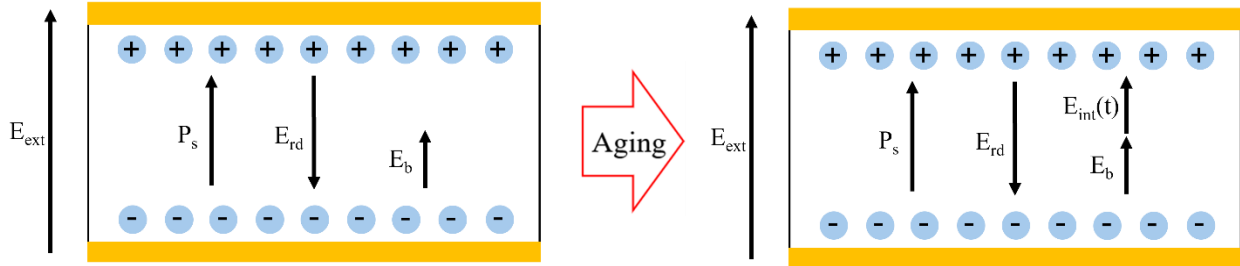


**Figure 11: Schematic of field dynamics that develop with HTPP**

The data and analysis in this study comprehensively link the rationale for the positive aging of the dielectric and electromechanical properties of these material systems. Phenomenological modeling has shown that this aging relaxation occurs within the framework of a far-from-equilibrium state which involves a time dependent internal field with minimal extrinsic contributions. Many questions still remain, including the microscopic and structural details of the state developing under pulse poling in conjunction with the defect dipole interactions that seemingly drive positive aging. The role of the internal field development in textured microstructures relative to single crystals is also not well understood, nor are the interfacial inhomogeneities that control the strain and displacement field distributions. Positive aging as well as general property enhancement that comes from pulse poling could raise new compositional design questions and opportunities to maximize these trends and internal field magnitudes.

#### 4. Conclusions

Mn-doped relaxor ferroelectrics have shown positive aging of piezoelectric and dielectric properties. Unlike typical aging, properties increased by 40-60% across the span of a month for the single crystals and 15-20% across a few weeks for the textured ceramics. This rise in properties coincided with internal field formation and intrinsic system changes. Transitions from ferroelectric to paraelectric phases upon heating no longer exhibited diffuse relaxor behavior after HTPP but appeared as a first-order phase transition. The non-equilibrium poling conditions brought on by pulse poling are believed to have left an unscreened depolarization field in the material which suppressed initial properties. With time, this was counteracted by the creation of an internal field due to defect dipole alignment. Differences in DSC signatures and X-ray diffraction patterns indicate the intrinsic nature of positive aging. Landau Theory provided a phenomenological explanation for this behavior, accurately describing the interdependent properties.

## 5. Supplemental Material:

### 5.1 Full derivation of elastic Gibbs free energy:

For simplicity, we shall omit tensor notation in the following derivations. The fundamental relation between elastic Gibbs and Helmholtz free energies is given by:

$$G(T, X, P) = F(T, x, P) - xX \quad (\text{S5.1})$$

Where  $G$  is Gibbs free energy,  $T$  is temperature,  $X$  is stress,  $x$  is strain,  $P$  is polarization, and  $F$  is Helmholtz free energy.  $F$  can be expressed via:

$$F(T, x, P) = F_1(T, P) + F_2(x) + F_3(x, P) \quad (\text{S5.2})$$

where  $F_1(T, P)$  is the Helmholtz Free energy given by the Landau theory,  $F_2(x)$  is the elastic energy, and  $F_3(x, P)$  is the interaction or coupling energy between the polarization and the spontaneous strain. Substituting this into Equation S5.1 gives:

$$G(T, X, P) = \frac{1}{2}\alpha P^2 + \frac{1}{4}\beta P^4 + \frac{1}{6}\gamma P^6 + \frac{1}{2}cx^2 + QxP^2 - xX \quad (\text{S5.3})$$

where  $c$  is the elastic stiffness,  $Q$  is the electrostrictive coefficient, and  $\alpha$ ,  $\beta$ , and  $\gamma$  are the Landau coefficients. To solve for the strain,  $x$ , one then takes the derivative of  $G$  with respect to  $x$  which is set equal to 0 for the equilibrium condition using the minimal principle. Once  $x$  is found, it can be inserted back into the original expression for  $G$ , which is now in its natural variables. This process is shown by:

$$\frac{dG}{dx} = cx + QP^2 - X = 0 \quad (\text{S5.4})$$

$$x = \frac{X - QP^2}{c} \quad (\text{S5.5})$$

$$G = \frac{1}{2}\left(\alpha + \frac{Q}{c}X\right)P^2 + \frac{1}{4}\left(\beta - \frac{Q^2}{2c}\right)P^4 + \frac{1}{6}\gamma P^6 - \frac{X^2}{2c} \quad (\text{S5.6})$$

Within the experiment considerations of a stress-free crystal as was used in this study,  $X = 0$ . So, the electrostrictive coupling will only impact the quadric term of the Landau expression, and this term as introduced in the text impacts the nature of the order of the phase transition.

### 5.2. Full derivation of effective piezoelectric coefficient:

The equation for strain as it relates to polarization is given by:

$$x = Q(P_{ind} + P_s)^2 \quad (\text{S5.7})$$

$$x = Q(P_{ind}^2 + 2P_s P_{ind} + P_s^2) \quad (S5.8)$$

where  $x$  is strain,  $Q$  is again the electrostrictive coefficient,  $P_s$  is spontaneous polarization and  $P_{ind}$  is the induced polarization. The expression can be further expanded using the relation for  $P_{ind}$  ( $P_{ind} = \epsilon_r \epsilon_0 E$ ) which yields:

$$x = Q(\epsilon_0^2 \epsilon_r^2 E^2 + 2\epsilon_0 \epsilon_r P_s E + P_s^2) \quad (S5.9)$$

$$x = Q\epsilon_0^2 \epsilon_r^2 E^2 + 2Q\epsilon_0 \epsilon_r P_s E + QP_s^2 \quad (S5.10)$$

where  $E$  is an applied electric field, which in most cases can be ignored. However, here  $E$  will be taken into consideration given the fact that there is an internal field ( $E_{int}$ ) developing in the material. With this and the fact that  $d_{eff}$  is equivalent to taking the derivative of  $x$  with respect to  $E$ , we yield the following:

$$x = ME^2 + 2Q\epsilon_0 \epsilon_r P_s E + QP_s^2 \quad (S5.11)$$

$$d_{eff} = \frac{dx}{dE} = 2ME_{int} + 2Q\epsilon_r \epsilon_0 P_s \quad (S5.12)$$

where  $M$  is the field dependent electrostrictive constant related to  $Q$  via  $M = Q\epsilon_0^2 \epsilon_r^2$ .

### 5.3. Strain vs. P<sup>2</sup> Plot

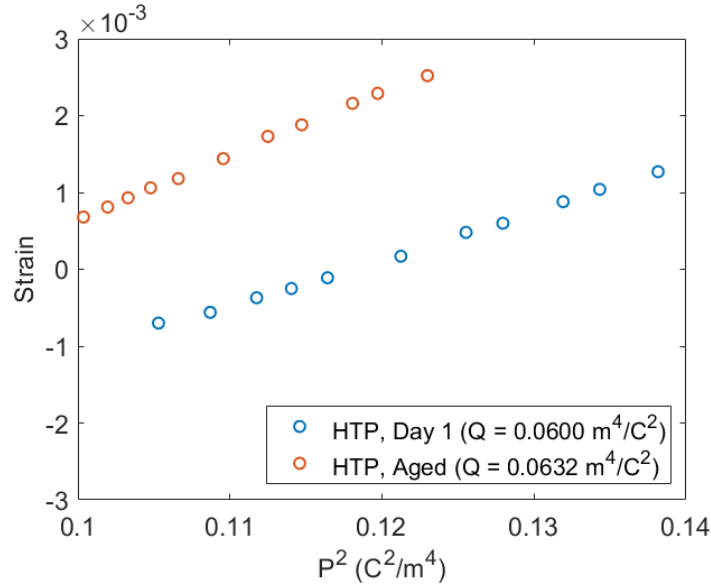


**Figure S1: Strain vs. P<sup>2</sup> plot for Mn: PIN-PMN-PT using data from the P-E and strain-field hysteresis loops.**

## 6. Acknowledgements

This material is based upon work supported by the National Science Foundation, as part of the Center for Dielectrics and Piezoelectrics under Grant Nos. IIP-1841453 and IIP-1841466. We would also like to thank TRS Technologies, Inc. and the Applied Research Lab for supplying the single crystal and textured samples respectively.

The authors would also like to thank Jeff Long, Michael Norrell, Steve Perini, and Dean Anderson at the Materials Research Institute of Penn State for their assistance in experimental setup and data extraction.

In reading and citing Ekhard Salje's papers considering the phenomenological description of the data, we acknowledged and would like to honor the memory of Ekhard who recently passed earlier this year.

## 7. References

- [1] L. E. Cross, "Ferroelectric materials for electromechanical transducer applications," 1996.
- [2] S. I. Shkuratov and C. S. Lynch, "A review of ferroelectric materials for high power devices," *Journal of Materiomics*, vol. 8, no. 4, pp. 739–752, Jul. 2022, doi: 10.1016/j.jmat.2022.04.002.
- [3] T. R. ShROUT and J. Fielding, "Relaxor Ferroelectric Materials."
- [4] A. A. Bokov and Z. G. Ye, "Recent progress in relaxor ferroelectrics with perovskite structure," *J Mater Sci*, vol. 41, no. 1, pp. 31–52, Jan. 2006, doi: 10.1007/s10853-005-5915-7.
- [5] L. E. Cross, "Relaxor ferroelectrics," *Ferroelectrics*, vol. 76, no. 1, pp. 241–267, 1987, doi: 10.1080/00150198708016945.
- [6] C. A. Randall, A. S. Bhalla, T. R. ShROUT, and L. E. Cross, "Classification and consequences of complex lead perovskite ferroelectrics with regard to B-site cation order," *J Mater Res*, vol. 5, no. 4, pp. 829–834, Apr. 1990, doi: 10.1557/JMR.1990.0829.
- [7] N. Setter and L. E. Cross, "The role of B-site cation disorder in diffuse phase transition behavior of perovskite ferroelectrics," *J Appl Phys*, vol. 51, no. 8, pp. 4356–4360, Aug. 1980, doi: 10.1063/1.328296.
- [8] A. Kumar *et al.*, "Atomic-resolution electron microscopy of nanoscale local structure in lead-based relaxor ferroelectrics," *Nat Mater*, vol. 20, no. 1, pp. 62–67, Jan. 2021, doi: 10.1038/s41563-020-0794-5.
- [9] M. Xu, S. Wei, C. Cem Tasan, and J. M. LeBeau, "Quantifying Chemical and Structural Order in Scanning Transmission Electron Microscopy (STEM) Datasets Using Spatial Statistics," *Microscopy and Microanalysis*, vol. 29, no. Supplement\_1, pp. 1986–1987, Jul. 2023, doi: 10.1093/micmic/ozad067.1029.

- [10] K. Rabe, C. Ahn, and J.-M. Triscone, *Physics of Ferroelectrics: A Modern Perspective*. Springer-Verlag Berlin Heidelberg, 2007.
- [11] V. A. Bokov and I. E. Mylnikova, "Electrical and optical properties of single crystals of ferroelectrics with a diffused phase transition," *Soviet Physics - Solid State*, vol. 3, no. 3, pp. 613–623, 1961.
- [12] J. C. M'Peko, A. G. Peixoto, E. Jiménez, and L. M. Gaggero-Sager, "Electrical properties of Nb-doped PZT 65/35 ceramics: Influence of Nb and excess PbO," *J Electroceram*, vol. 15, no. 2, pp. 167–176, Nov. 2005, doi: 10.1007/s10832-005-2403-z.
- [13] K. Uchino, S. Nomura, L. E. Cross, R. E. Newnham, and S. J. Jang, "Review Electrostrictive effect in perovskites and its transducer applications," 1981.
- [14] Seung-Eek Park and T. R. Shrout, "Characteristics of relaxor-based piezoelectric single crystals for ultrasonic transducers," *IEEE Trans Ultrason Ferroelectr Freq Control*, vol. 44, no. 5, pp. 1140–1147, Sep. 1997, doi: 10.1109/58.655639.
- [15] C. A. Randall, A. Kelnberger, G. Y. Yang, R. E. Eitel, and T. R. Shrout, "High Strain Piezoelectric Multilayer Actuators? A Material Science and Engineering Challenge," *J Electroceram*, vol. 14, no. 3, pp. 177–191, Jul. 2005, doi: 10.1007/s10832-005-0956-5.
- [16] K. Uchino, *Ferroelectric Devices*. Boca Raton: Taylor and Francis Group, 2018.
- [17] L. Bian *et al.*, "High-Performance [001]c-Textured PNN-PZT Relaxor Ferroelectric Ceramics for Electromechanical Coupling Devices," *Adv Funct Mater*, vol. 30, no. 25, Jun. 2020, doi: 10.1002/adfm.202001846.
- [18] B. H. Watson, M. J. Brova, M. Fanton, R. J. Meyer, and G. L. Messing, "Textured Mn-doped PIN-PMN-PT Ceramics: Harnessing Intrinsic Piezoelectricity for High-power Transducer Applications," *J Eur Ceram Soc*, vol. 41, no. 2, pp. 1270–1279, Feb. 2021, doi: 10.1016/j.jeurceramsoc.2020.07.071.
- [19] Y. Chen *et al.*, "High-frequency PIN-PMN-PT single crystal ultrasonic transducer for imaging applications," *Applied Physics A*, vol. 108, no. 4, pp. 987–991, Sep. 2012, doi: 10.1007/s00339-012-7009-0.
- [20] Jie Chen and R. Panda, "Review: commercialization of piezoelectric single crystals for medical imaging applications," in *IEEE Ultrasonics Symposium, 2005.*, IEEE, pp. 235–240. doi: 10.1109/ULTSYM.2005.1602839.
- [21] R. E. Cohen, "Origin of ferroelectricity in perovskite oxides," *Nature*, vol. 358, no. 6382, pp. 136–138, Jul. 1992, doi: 10.1038/358136a0.
- [22] C. M. Fancher *et al.*, "The contribution of 180° domain wall motion to dielectric properties quantified from in situ X-ray diffraction," *Acta Mater*, vol. 126, pp. 36–43, Mar. 2017, doi: 10.1016/j.actamat.2016.12.037.
- [23] S. I. Shkuratov and C. S. Lynch, "A review of ferroelectric materials for high power devices," *Journal of Materiomics*, vol. 8, no. 4, pp. 739–752, Jul. 2022, doi: 10.1016/j.jmat.2022.04.002.

- [24] G. H. Haertling, "Ferroelectric ceramics: History and technology," *Journal of the American Ceramic Society*, vol. 82, no. 4, pp. 797–818, 1999, doi: 10.1111/j.1151-2916.1999.tb01840.x.
- [25] H. Jaffe, "Piezoelectric Ceramics," *Journal of the American Ceramic Society*, vol. 41, no. 11, pp. 494–498, 1958, doi: 10.1111/j.1151-2916.1958.tb12903.x.
- [26] M. Habib, I. Lantgios, and K. Hornbostel, "A review of ceramic, polymer and composite piezoelectric materials," Oct. 20, 2022, *Institute of Physics*. doi: 10.1088/1361-6463/ac8687.
- [27] J. F. Tressler, S. Alkoy, and R. E. Newnham, "Piezoelectric Sensors and Sensor Materials," 1998.
- [28] H. Yu, V. Gopalan, J. Sindel, and C. A. Randall, "Domain switching and electromechanical properties of pulse poled  $\text{Pb}(\text{Zn}_{1/3}\text{Nb}_{2/3})\text{O}_3\text{-PbTiO}_3$  crystals," *J Appl Phys*, vol. 89, no. 1, pp. 561–567, Jan. 2001, doi: 10.1063/1.1289221.
- [29] V. Y. Shur, A. R. Akhmatkhanov, and I. S. Baturin, "Micro- and nano-domain engineering in lithium niobate," Dec. 01, 2015, *American Institute of Physics Inc.* doi: 10.1063/1.4928591.
- [30] H. Yu and C. A. Randall, "Dendritic domain configurations in  $\text{Pb}(\text{Zn}_{1/3}\text{Nb}_{2/3})\text{O}_3\text{-PbTiO}_3$  single crystals," *J Appl Phys*, vol. 86, no. 10, pp. 5733–5738, Nov. 1999, doi: 10.1063/1.371586.
- [31] J. Xiong *et al.*, "Performance enhancement of  $\text{Pb}(\text{In}_{1/2}\text{Nb}_{1/2})\text{O}_3\text{-PbTiO}_3$  ferroelectric single crystals using pulse poling," *Scr Mater*, vol. 215, Jul. 2022, doi: 10.1016/j.scriptamat.2022.114694.
- [32] S. Chen *et al.*, "Achieving high piezoelectric performance in  $\text{Pb}(\text{Mg}_{1/3}\text{Nb}_{2/3})\text{O}_3\text{-PbTiO}_3$  ferroelectric single crystals through pulse poling technique," *J Appl Phys*, vol. 136, no. 16, Oct. 2024, doi: 10.1063/5.0234048.
- [33] P. V Lambeck and G. H. Jonker, "The Nature of Domain Stabilization in Ferroelectric Perovskites," 1986.
- [34] D. Zhao *et al.*, "Depolarization of multidomain ferroelectric materials," *Nat Commun*, vol. 10, no. 1, p. 2547, Jun. 2019, doi: 10.1038/s41467-019-10530-4.
- [35] A. K. Tagantsev, I. Stolichnov, E. L. Colla, and N. Setter, "Polarization fatigue in ferroelectric films: Basic experimental findings, phenomenological scenarios, and microscopic features," *J Appl Phys*, vol. 90, no. 3, pp. 1387–1402, Aug. 2001, doi: 10.1063/1.1381542.
- [36] Y. Yu, Z. Qin, X. Zhang, Y. Chen, G. Qin, and S. Li, "Far-From-Equilibrium Processing Opens Kinetic Paths for Engineering Novel Materials by Breaking Thermodynamic Limits," *ACS Mater Lett*, vol. 7, no. 1, pp. 319–332, Jan. 2025, doi: 10.1021/acsmaterialslett.4c01952.
- [37] Q. M. Zhang, J. Zhao, and L. E. Cross, "Aging of the dielectric and piezoelectric properties of relaxor ferroelectric lead magnesium niobate-lead titanate in the electric field biased state," *J Appl Phys*, vol. 79, no. 6, pp. 3181–3187, Mar. 1996, doi: 10.1063/1.361261.

- [38] J. H. Koh, S. J. Jeong, M. S. Ha, and J. S. Song, "Aging of piezoelectric properties in  $\text{Pb}(\text{MgNb})\text{O}_3\text{-Pb}(\text{ZrTi})\text{O}_3$  multilayer ceramic actuators," *J Appl Phys*, vol. 96, no. 1, pp. 544–548, Jul. 2004, doi: 10.1063/1.1755437.
- [39] R. Herbiet, H. Tenbrock, and G. Arlt, "The aging behaviour of the complex material parameters  $\epsilon$ ,  $d$  and  $s$  in ferroelectric PZT ceramics," *Ferroelectrics*, vol. 76, no. 1, pp. 319–326, Dec. 1987, doi: 10.1080/00150198708016952.
- [40] K. W. Plessner, "Ageing of the Dielectric Properties of Barium Titanate Ceramics," *Proceedings of the Physical Society. Section B*, vol. 69, no. 12, pp. 1261–1268, Dec. 1956, doi: 10.1088/0370-1301/69/12/309.
- [41] P. V. Lambeck and G. H. Jonker, "Ferroelectric domain stabilization in  $\text{BaTiO}_3$  by bulk ordering of defects," *Ferroelectrics*, vol. 22, no. 1, pp. 729–731, Jan. 1978, doi: 10.1080/00150197808237382.
- [42] G. Williams and D. C. Watts, "Non-symmetrical dielectric relaxation behaviour arising from a simple empirical decay function," *Transactions of the Faraday Society*, vol. 66, p. 80, 1970, doi: 10.1039/tf9706600080.
- [43] R. Kohlrausch, "Theorie des elektrischen Rückstandes in der Leidener Flasche," *Ann Phys*, vol. 167, no. 1, pp. 56–82, Jan. 1854, doi: 10.1002/andp.18541670103.
- [44] J. C. Phillips, "Stretched exponential relaxation in molecular and electronic glasses," *Reports on Progress in Physics*, vol. 59, no. 9, pp. 1133–1207, Sep. 1996, doi: 10.1088/0034-4885/59/9/003.
- [45] L. Luo, M. Dietze, C. H. Solterbeck, H. Luo, and M. Es-Souni, "Tuning the functional properties of PMN-PT single crystals via doping and thermoelectrical treatments," *J Appl Phys*, vol. 114, no. 22, Dec. 2013, doi: 10.1063/1.4847975.
- [46] E. Sun, R. Zhang, F. Wu, B. Yang, and W. Cao, "Influence of manganese doping to the full tensor properties of  $0.24\text{Pb}(\text{In}_{1/2}\text{Nb}_{1/2})\text{O}_3\text{-}0.47\text{Pb}(\text{Mg}_{1/3}\text{Nb}_{2/3})\text{O}_3\text{-}0.29\text{PbTiO}_3$  single crystals," *J Appl Phys*, vol. 113, no. 7, Feb. 2013, doi: 10.1063/1.4792600.
- [47] H. Hoshyarmanesh and Y. Maddahi, "Poling Process of Composite Piezoelectric Sensors for Structural Health Monitoring: A Pilot Comparative Study," *IEEE Sens Lett*, vol. 2, no. 1, pp. 1–4, Mar. 2018, doi: 10.1109/LSENS.2018.2806301.
- [48] R. G. Polcawich and S. Trolier-McKinstry, "Piezoelectric and dielectric reliability of lead zirconate titanate thin films," *J Mater Res*, vol. 15, no. 11, pp. 2505–2513, 2000, doi: 10.1557/JMR.2000.0360.
- [49] J. G. P. Holterman, *Introduction to Piezoelectric Materials and Components*. Apeldoorn: Stichting Applied Piezo, 2012.
- [50] D. Damjanovic and M. Demartin, "The Rayleigh law in piezoelectric ceramics," *J Phys D Appl Phys*, vol. 29, no. 7, pp. 2057–2060, Jul. 1996, doi: 10.1088/0022-3727/29/7/046.

- [51] D. A. Hall, "Rayleigh behaviour and the threshold field in ferroelectric ceramics," *Ferroelectrics*, vol. 223, no. 1, pp. 319–328, Mar. 1999, doi: 10.1080/00150199908260586.
- [52] C. B. Sawyer and C. H. Tower, "Rochelle Salt as a Dielectric," *Physical Review*, vol. 35, no. 3, pp. 269–273, Feb. 1930, doi: 10.1103/PhysRev.35.269.
- [53] D. Zhang, H. Wu, C. R. Bowen, and Y. Yang, "Recent Advances in Pyroelectric Materials and Applications," *Small*, vol. 17, no. 51, Dec. 2021, doi: 10.1002/sml.202103960.
- [54] R. Ghane-Motlagh, M. Kroener, F. Goldschmidtboeing, A. N. Danilewsky, and P. Woias, "A dynamic method for the measurement of pyroelectric properties of materials," *Smart Mater Struct*, vol. 27, no. 8, p. 084004, Aug. 2018, doi: 10.1088/1361-665X/aac0b3.
- [55] A. Barzegar, R. Bagheri, and A. Karimi Taheri, "Aging of piezoelectric composite transducers," *J Appl Phys*, vol. 89, no. 4, pp. 2322–2326, Feb. 2001, doi: 10.1063/1.1339853.
- [56] Y. A. Genenko, J. Glaum, M. J. Hoffmann, and K. Albe, "Mechanisms of aging and fatigue in ferroelectrics," *Materials Science and Engineering: B*, vol. 192, pp. 52–82, Feb. 2015, doi: 10.1016/j.mseb.2014.10.003.
- [57] W. P. Mason, "Aging of the Properties of Barium Titanate and Related Ferroelectric Ceramics," *J Acoust Soc Am*, vol. 27, no. 1, pp. 73–85, Jan. 1955, doi: 10.1121/1.1907500.
- [58] Y. Yan, K.-H. Cho, and S. Priya, "Piezoelectric properties and temperature stability of Mn-doped  $\text{Pb}(\text{Mg}_{1/3}\text{Nb}_{2/3})\text{-PbZrO}_3\text{-PbTiO}_3$  textured ceramics," *Appl Phys Lett*, vol. 100, no. 13, Mar. 2012, doi: 10.1063/1.3698157.
- [59] Y. Chang *et al.*, "Grain-Oriented Ferroelectric Ceramics with Single-Crystal-like Piezoelectric Properties and Low Texture Temperature," *ACS Appl Mater Interfaces*, vol. 12, no. 34, pp. 38415–38424, Aug. 2020, doi: 10.1021/acsami.0c11680.
- [60] G. Karas, *Trends in Crystal Growth Research*. Nova Science Pub, Inc., 2005.
- [61] J. Glaum, Y. A. Genenko, H. Kungl, L. Ana Schmitt, and T. Granzow, "De-aging of Fe-doped lead-zirconate-titanate ceramics by electric field cycling: 180°- vs. non-180° domain wall processes," *J Appl Phys*, vol. 112, no. 3, Aug. 2012, doi: 10.1063/1.4739721.
- [62] M. Ju *et al.*, "Evolving electromechanical properties of defect engineered  $\text{Pb}(\text{Zr,Ti})\text{O}_3$ -based piezoceramics," *Next Materials*, vol. 1, no. 4, p. 100043, Dec. 2023, doi: 10.1016/j.nxmate.2023.100043.
- [63] H. Funakubo, M. Dekkers, A. Sambri, S. Gariglio, I. Shklyarevskiy, and G. Rijnders, "Epitaxial PZT films for MEMS printing applications," *MRS Bull*, vol. 37, no. 11, pp. 1030–1038, Nov. 2012, doi: 10.1557/mrs.2012.271.
- [64] R. E. Eitel, T. R. Shrout, and C. A. Randall, "Nonlinear contributions to the dielectric permittivity and converse piezoelectric coefficient in piezoelectric ceramics," *J Appl Phys*, vol. 99, no. 12, Jun. 2006, doi: 10.1063/1.2207738.

- [65] R. Birjega, A. Andrei, M. Dinescu, F. Craciun, and C. Galassi, "Phase Transitions, Dielectric and Ferroelectric Properties of Lead-free NBT-BT Thin Films," in *Advances in Ferroelectrics*, InTech, 2012. doi: 10.5772/52395.
- [66] M. C. Shin, S. J. Chung, S.-G. Lee, and R. S. Feigelson, "Growth and observation of domain structure of Lead Magnesium Niobate–Lead Titanate Single Crystals," *J Cryst Growth*, vol. 263, no. 1–4, pp. 412–420, Mar. 2004, doi: 10.1016/j.jcrysgr.2003.12.024.
- [67] M. Ma, S. Xia, K. Song, H. Guo, Z. Xu, and Z. Li, "Enhanced transverse piezoelectric properties by composition and poling electric field induced phase transition in PIN–PMN–PT single crystal near morphotropic phase boundary," *J Appl Phys*, vol. 130, no. 6, Aug. 2021, doi: 10.1063/5.0055416.
- [68] C. He, T. Karaki, X. Yang, Y. (John) Yamashita, Y. Sun, and X. Long, "Dielectric and piezoelectric properties of  $\text{Pb}[(\text{Mg}_{1/3}\text{Nb}_{2/3})_{0.52}(\text{Yb}_{1/2}\text{Nb}_{1/2})_{0.15}\text{Ti}_{0.33}]\text{O}_3$  single-crystal rectangular plate and beam mode transducers poled by alternate current poling," *Jpn J Appl Phys*, vol. 58, no. SL, p. SLLD06, Nov. 2019, doi: 10.7567/1347-4065/ab37b7.
- [69] Y. Sun, T. Karaki, and Y. Yamashita, "Recent progress on AC poling of relaxor-PbTiO<sub>3</sub> ferroelectric single crystals: a review," *Jpn J Appl Phys*, vol. 61, no. SB, p. SB0802, Feb. 2022, doi: 10.35848/1347-4065/ac3a90.
- [70] D. Vanderbilt and M. H. Cohen, "Monoclinic and triclinic phases in higher-order Devonshire theory," *Phys Rev B*, vol. 63, no. 9, p. 094108, Jan. 2001, doi: 10.1103/PhysRevB.63.094108.
- [71] H.-P. Kim *et al.*, "Poling-free relaxor-PbTiO<sub>3</sub> single crystals," *Journal of Materiomics*, vol. 11, no. 3, p. 100887, May 2025, doi: 10.1016/j.jmat.2024.05.002.
- [72] A. M. Glass, "Investigation of the Electrical Properties of  $\text{Sr}_{1-x}\text{Ba}_x\text{Nb}_2\text{O}_6$  with Special Reference to Pyroelectric Detection," *J Appl Phys*, vol. 40, no. 12, pp. 4699–4713, Nov. 1969, doi: 10.1063/1.1657277.
- [73] C. De, S. Ghara, and A. Sundaresan, "Effect of internal electric field on ferroelectric polarization in multiferroic TbMnO<sub>3</sub>," *Solid State Commun*, vol. 205, pp. 61–65, Mar. 2015, doi: 10.1016/j.ssc.2015.01.002.
- [74] S. Pandya *et al.*, "Pyroelectric energy conversion with large energy and power density in relaxor ferroelectric thin films," *Nat Mater*, vol. 17, no. 5, pp. 432–438, May 2018, doi: 10.1038/s41563-018-0059-8.
- [75] D. Li and S.-G. Lu, "Electrocaloric Effect and Phase Transitions in Ferroelectrics," *International Journal of Metallurgical & Materials Engineering*, vol. 4, no. 141, 2018.
- [76] M. Iqbal Khan and T. Chandra Upadhyay, "General Introduction to Ferroelectrics," in *Multifunctional Ferroelectric Materials*, IntechOpen, 2021. doi: 10.5772/intechopen.97720.
- [77] V. Ginzburg and L. Landau, "On The Theory of Superconductivity," *Zh.Eksp.Teor.Fiz.*, vol. 20, pp. 1064–1082, 1950.

- [78] A. F. Devonshire, "Theory of barium titanate," *The London, Edinburgh, and Dublin Philosophical Magazine and Journal of Science*, vol. 40, no. 309, pp. 1040–1063, Oct. 1949, doi: 10.1080/14786444908561372.
- [79] S. Lee, G. A. Rossetti, Z.-K. Liu, and C. A. Randall, "Intrinsic ferroelectric properties of the nonstoichiometric perovskite oxide  $\text{Ba}_{1-x}\text{Ti}_{1-y}\text{O}_{3-x-2y}$ ," *J Appl Phys*, vol. 105, no. 9, May 2009, doi: 10.1063/1.3109210.
- [80] E. K. H. Salje, "Crystallography and structural phase transitions, an introduction," *Acta Crystallogr A*, vol. 47, no. 5, pp. 453–469, Sep. 1991, doi: 10.1107/S0108767391004300.
- [81] F. Guillou *et al.*, "Non-hysteretic first-order phase transition with large latent heat and giant low-field magnetocaloric effect," *Nat Commun*, vol. 9, no. 1, p. 2925, Jul. 2018, doi: 10.1038/s41467-018-05268-4.
- [82] W. J. Merz, "Double Hysteresis Loop of  $\text{BaTiO}_3$  at the Curie Point," *Physical Review*, vol. 91, no. 3, pp. 513–517, Aug. 1953, doi: 10.1103/PhysRev.91.513.
- [83] C. L. Wang and S. R. P. Smith, "Landau theory of the size-driven phase transition in ferroelectrics," *Journal of Physics: Condensed Matter*, vol. 7, no. 36, pp. 7163–7171, Sep. 1995, doi: 10.1088/0953-8984/7/36/006.
- [84] M. Stewart, M. Cain, and D. Hall, *Ferroelectric Hysteresis Measurements and Analysis*. Teddington: National Physical Laboratory, 1999.
- [85] L. Jin, F. Li, and S. Zhang, "Decoding the Fingerprint of Ferroelectric Loops: Comprehension of the Material Properties and Structures," *Journal of the American Ceramic Society*, vol. 97, no. 1, pp. 1–27, Jan. 2014, doi: 10.1111/jace.12773.
- [86] R. A. Maier, T. A. Pomorski, P. M. Lenahan, and C. A. Randall, "Acceptor-oxygen vacancy defect dipoles and fully coordinated defect centers in a ferroelectric perovskite lattice: Electron paramagnetic resonance analysis of  $\text{Mn}^{2+}$  in single crystal  $\text{BaTiO}_3$ ," *J Appl Phys*, vol. 118, no. 16, Oct. 2015, doi: 10.1063/1.4934505.
- [87] G. Arlt and H. Neumann, "Internal bias in ferroelectric ceramics: Origin and time dependence," *Ferroelectrics*, vol. 87, no. 1, pp. 109–120, Nov. 1988, doi: 10.1080/00150198808201374.